JST: Engineering and Technology for Sustainable Development
Volume 35, Issue 2, April 2025, 001-008

A Comparative Study on the Structure and Photoactivity of Titanium Dioxide Obtained from Various Synthetics for the Degradation of Organic Dye

Nguyen Quynh Vi, Dinh Ngoc Duong, Nguyen Thanh Hung, Truong Minh Thu, Le Minh Thang, Nguyen Ngoc Mai*

Hanoi University of Science and Technology, Ha Noi, Vietnam
**Corresponding author email: mai.nguyenngoc@hust.edu.vn*

Abstract

Titanium dioxide (TiO_2) particles were synthesized by the sol-gel method (SG) and sol-gel low-temperature method (SG-L), utilizing titanium isopropoxide as the precursor. Subsequently, the particles underwent heat treatment with sodium hydroxide 10M, resulting in samples denoted as SG-H and SG-L-H samples, respectively. The purpose of this study is to compare these synthesis methods in terms of the stability and photocatalytic activity of TiO_2 catalysts. To determine the optimal synthesis method for generating highly active TiO_2, the obtained catalyst samples were characterized by a variety of techniques, including thermogravimetric analysis (TGA), differential scanning calorimetry (DSC), X-ray diffraction (XRD), Brunauer-Emmett-Teller (BET), and UV-vis spectroscopy measurements. The results demonstrated that the structure and phase of catalysts depend on the synthesis conditions. The surface area measurements indicated values of 0.95, 18.95, 82.65, and 168.59 m^2/g for SG, SG-H, SG-L, and SG-L-H, respectively. Furthermore, the degradation efficiency of methylene blue under xenon lamp illumination was recorded at 87%, 91%, 97%, and 94% after 150 minutes, according to a pseudo-first-order reaction. These results suggest that the sol-gel low-temperature method is particularly effective in producing high purity, large specific surface area, and good decomposition of organic dye.

Keywords: Hydrothermal, sol-gel, sol-gel low-temperature, TiO_2 particles.

1. Introduction

Titanium dioxide (TiO_2) is one of the most significant nanomaterials that has received a lot of interest because of its wide applications. In particular, TiO_2 has demonstrated tremendous potential in photocatalysts because of its chemical stability and lack of toxicity [1]. TiO_2 has three phases including brookite, anatase, and rutile. The anatase phase has the ability to decolorize faster than the other phases [2]. Therefore, many researchers focus on the synthesis of high-purity anatase TiO_2 catalysts.

There are many methods to synthesize anatase TiO_2 catalyst materials, such as the sol-gel method, hydrothermal method, precipitation method, etc. The process of synthesizing nanomaterials by the sol-gel method includes four steps: hydrolysis, polycondensation, drying, and thermal decomposition [3]. This is a common method for the synthesis of metallic oxides and mixtures of metallic oxides. Although the obtained material has high homogeneity and purity, its bond formation and wear resistance are not good [4]. Another method is hydrothermal, which has been illustrated to be very efficient and convenient for the preparation of TiO_2 and exhibits good catalytic activity for dye degradation [5]. In comparison to the sol-gel method, the hydrothermal method-generated photocatalyst has a higher crystallinity, greater surface area, and stronger absorption [5]. However, the hydrothermal method uses chemicals at high concentrations and high temperatures for a long time, which is expensive for materials and harmful to the environment. Thus, there are some restrictions on traditional synthesis. Therefore, a number of studies have been conducted to investigate the optimal TiO_2 synthesis conditions that can achieve the highest degradation efficiency [1]. However, there is a lack of studies comparing the effects of synthesis conditions on the TiO_2 phase and its activity.

This work presents the synthesis and characterization of TiO_2 nanoparticles prepared by the sol-gel method (SG) and sol-gel low-temperature (SG-L) from titanium isopropoxide (TTIP) precursor. In addition, SG and SG-L samples were further treated using the hydrothermal method to evaluate their stability. The aim of our research is to compare the structure and photoactivity of TiO_2 particles obtained from these methods for the degradation of organic dye using methylene blue (MB) as a target pollutant. The crystallinity and phase identification were examined by X-ray diffraction (XRD). The scanning electron

ISSN 2734-9381
https://doi.org/10.51316/jst.181.etsd.2025.35.2.1
Received: Aug 28, 2024; revised: Dec 9, 2024
accepted: Dec 10, 2024

microscopy (SEM) analysis showed the morphology of TiO_2 nanoparticles while the energy dispersive X-ray spectroscopy (EDX) analysis showed the elemental composition. The comparison of the characterization of samples was determined by Thermogravimetric Analysis (TGA), Differential Scanning Calorimetry (DSC), and Brunauer-Emmett-Teller (BET). The activity of the catalyst was evaluated through its ability to degrade MB in order to find an optimal method of TiO_2 synthesis. Finally, the kinetics of MB removal were studied.

2. Materials and Methods

2.1. Materials

Titanium isopropoxide (TTIP, 97%), Sodium hydroxide (NaOH, pellets, ≥ 98%), and Acetic acid (CH_3COOH, > 99%) were purchased from Sigma Aldrich. Nitric acid (HNO_3, 69%), Methylene blue (MB), and Hydrochloric acid (HCl, 37%) were provided by Merck. Ethanol absolute (C_2H_6O, 99.7%) was obtained from GHTech, China.

2.2. Methods

2.2.1. The methods for the synthesis of TiO_2

Sol-gel method

The sol-gel method is commonly employed to synthesize TiO_2 due to its benefits, including high purity, relatively low processing temperatures, and the ability to control stoichiometry [6, 7]. The synthesis process in this study was as follows (Fig. 1): First, a sol-solution was obtained by slowly pouring the mixture containing ethanol and TTIP into distilled water. The pH of the solution was controlled at around 2 by HNO_3. In the next step, the sol-solution was agitated at room temperature for 4 hours to produce a white gel. After centrifuging, the obtained gel was dried at 120 °C for 8 hours. Finally, the gel was calcined at 800 °C for 5 hours with a heating rate of 5 °C/min to obtain TiO_2 particles, denoted as SG.

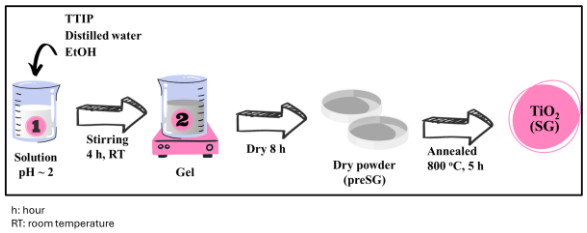

Fig. 1. Schematic overview of TiO_2 synthesis using sol-gel method (SG)

Sol-gel low-temperature method

In the recent years, the low-temperature sol-gel method has been developed for synthesizing TiO_2 [8]. TiO_2 particles in this research were prepared by the sol-gel low-temperature method, as shown in Fig. 2, and the synthesis process was as follows: First, the sol-solution was prepared by mixing TTIP, acetic acid, and distilled water at 0 to 5 °C. The reaction conditions were kept at a low temperature of about 5 °C. Then, the sol solution was stirred for 2 hours at room temperature to make a gel. After drying for 48 hours at 80 °C, the gel was crushed and then calcined at 450 °C for 5 hours at a heating rate of 2 °C/min. After synthesis, the TiO_2 photocatalyst was designated as SG-L.

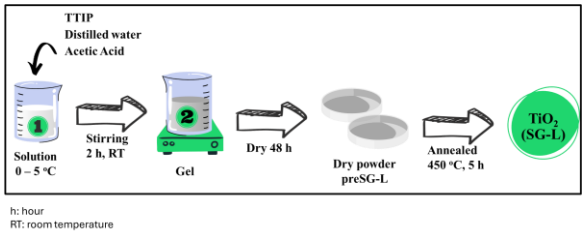

Fig. 2. Schematic overview of TiO_2 synthesis using sol-gel low-temperature method (SG-L)

Hydrothermal method

After synthesizing from the two mentioned processes (SG and SG-L), the catalyst powders were placed into a hydrothermal autoclave with a 10M NaOH solution and heated to 150 °C for 48 hours [9]. The resulting precipitate was washed with 1M HCl and distilled water. Finally, the catalyst was dried at 80 °C for 3 hours. As a result of the thermal destruction process conducted for each sample SG and SG-L, samples SG-H and SG-L-H were obtained. The hydrothermal procedure is summarized in Fig. 3.

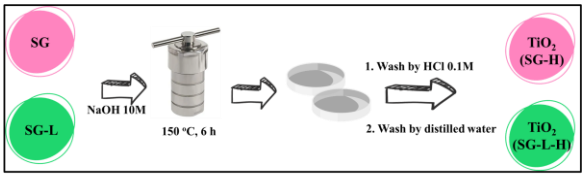

Fig. 3. Schematic overview of TiO_2 synthesis using hydrothermal method (SG-H and SG L-H)

2.2.2. The methods for characterization of TiO_2

Thermogravimetric analysis (TGA) and Differential Scanning Calorimetry (DSC) of the catalyst samples were performed using a NETZSCH STA 449F5 calorimetric analyzer in a temperature range of 25 °C - 450 °C for precursor, synthesized by the sol-gel low-temperature method and 25 °C - 850 °C for precursor, synthesized by the sol-gel method under an air stream at a heating rate of 1 °C/min.

X-ray diffraction (XRD) data was recorded under the conditions of Cu K_α radiation (40 kV, 35 mA) and XRD powder patterns were acquired on X'Pert Pro equipped (PANalytical) equipment. The crystallite size was determined from XRD data by the following Scherrer equation [10]:

$$D = \frac{k\lambda}{\beta.cos\theta} \quad (1)$$

where k is the Scherrer constant (close to 0.9), λ is the X-ray wavelength (nm) of Cu K_α, β is the full width at the half-maximum intensity of the peak in radians, and θ is the Bragg diffraction angle.

SEM on a JEOL JCM-7000 BENCHTOP SEM was used to analyze the morphology and structure of the catalyst particles.

In this study, the surface area of each sample was measured by the Brunauer-Emmett-Teller (BET) method on a Micromeritics Gemini VII 2390 analyzer.

The UV-Vis spectra of the samples were obtained using an Avantes UV-Vis spectrometer. For UV-Vis Diffuse Reflectance Spectroscopy (UV-DRS), the catalyst sample was analyzed. This technique employs $BaSO_4$ as a standard diffuse reflectance material to represent the absorption wavelength range of the catalysts. Consequently, the band gap of the samples was determined. Additionally, for UV-Vis measurements, a liquid sample of MB solution was utilized to assess the concentration of the MB solution before and after photocatalysis.

2.2.3. Investigation of the photocatalytic performance of TiO_2

The degradation of MB solution at 10 ppm (50 mL) was used to assess the photocatalytic capacity of the catalyst powder. Samples of 0.01 g TiO_2 powder were taken for the catalyst evaluation. To fully enable the absorption of the catalyst samples, the MB solution containing the catalyst was first agitated in the dark for 40 minutes. The mixture was then stirred for 2 hours while being illuminated. A 300 W xenon lamp that contained 5% UV light, was employed as the light source in this study since it emits visible radiation. Every 20 minutes, a solution sample was obtained, then all catalysts were centrifuged. Utilizing an Avantes UV-vis spectrometer, the absorbance at 664 nm was measured to determine the MB solution's concentration (C). A calibration curve can be used to determine the concentration of the MB solution. This approach's guiding principles adhere to the Lambert-Beer law [11]:

$$A = \varepsilon CL \quad (2)$$

where L is the length of the path, C is the concentration of the solution, and ε is the molar absorptivity (or extinction coefficient). We can calculate the MB degradation efficiency (DE) by the following formula [2]:

$$\text{DE (\%)} = \frac{C_0 - C_t}{C_t} \times 100 \quad (3)$$

in which C_0 is the initial concentration of MB (ppm), C_t is the concentration of MB at time t (ppm), and t is the contact time in minutes. The concentrations of the MB solution were determined by extrapolating the absorbance (A) at 664 nm using the calibration curve.

3. Results and Discussion

3.1. Characterization of Catalysts

To study the thermal transformation process and phase transition temperature during catalyst calcination, the dry powder samples before calcination were analyzed by using thermogravimetric (TGA). The samples used in this analysis were two dry powder samples before calcination: pre-SG (Fig. 4) and pre-SG-L (Fig. 5).

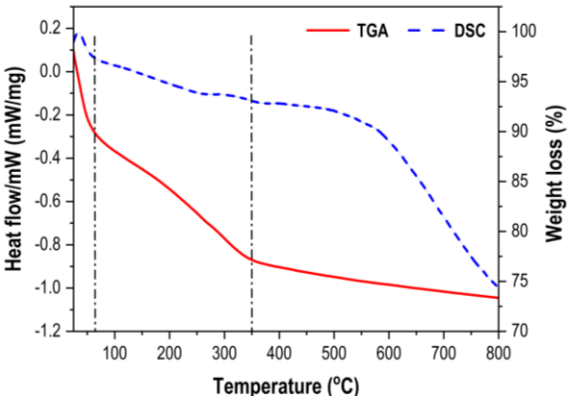

Fig. 4. TGA and DSC chart of pre-SG

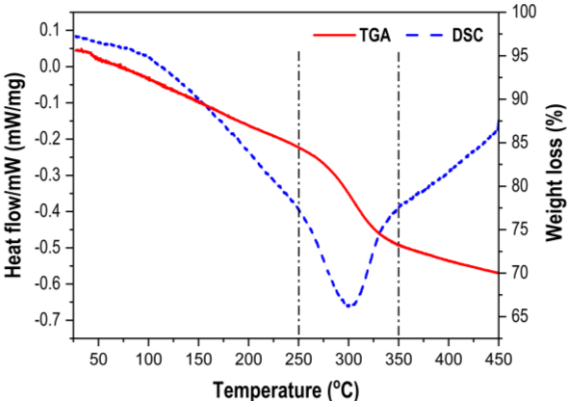

Fig. 5. TGA and DSC chart of pre-SG-L

For pre-SG, the TGA thermogram can be divided into three stages (Fig. 4), including first stage (50 - 70 °C), second stage (70 - 350 °C), and third stage (350 - 800 °C). In the first stage, there is a constant mass loss of about 12%. This is due to the removal of water from the titania gel. In the second stage, it can be seen the additional mass loss of 10%, and there is no peak in the DSC line. However, in the last stage, there is an exothermic peak at around 550 °C in the DSC thermogram and the mass loss is minor. It is supposed to be related to the transformation of the titania from anatase to the rutile phase [12]. Therefore, it can be assumed that at the second stage where there may have been an anatase phase formation at about

300 ºC [13], then when the calcination temperature increased to 800 ºC, the entire anatase phase transformed into the rutile phase.

The TGA thermogram for pre-SG-L is shown in Fig. 5 with 3 stages: from 50 ºC to 250 ºC, from 250 ºC to 350 ºC, and from 350 ºC to 450 ºC. A steady mass loss of 10% occurs in the first stage. The elimination of water from the titania gel is to blame for this. In the next stage, an additional 20% mass loss occurs and has an endothermic peak at 300 ºC in the DSC graph. It is assumed to be connected to the titania's transition from the amorphous to the anatase phase. In the final stage, there is little mass loss. Thus, it can be seen that the calcination temperature affects the formation of TiO_2 phases [14]. The anatase phase forms at around 300 °C, while the rutile phase forms at around 600 °C.

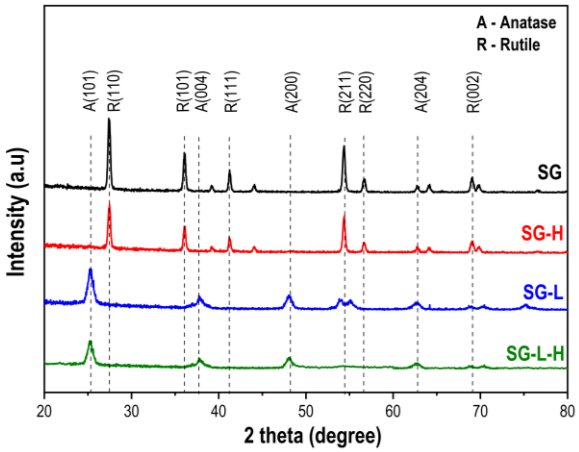

Fig. 6. The X-ray diffraction spectra of TiO_2, synthesized by the different methods

The X-ray diffraction (XRD) technique was employed to investigate the crystalline phases, crystal structure and purity of the synthesized TiO_2 samples in the scattering angle range ($20° \leq 2\theta \leq 80°$). The wide-angle X-ray scattering of the SG and SG-H samples exhibited diffraction peaks at 2θ positions of 27.45°, 36.1°, 41.2°, 54.4°, 56.6° and 69.1°, corresponding to the (110), (101), (111), (211), (220), and (002) planes, respectively. The strong intensity at 27.45° indicated good crystallization, characteristic of the rutile phase and the diffraction peaks matched with the Joint Committee on Powder Diffraction Standard (JCPDS) card number 21-1276. On the other hand, the X-ray diffraction patterns of the SG-L and SG-L-H samples revealed diffraction peaks characteristic of the anatase phase. The strong X-ray diffraction intensity at 25.32° corresponded to the (101) plane, indicating the formation of the tetragonal TiO_2 anatase phase and the diffraction peaks agreed with the JCPDS card number 21-1272. No diffraction peaks related to impurities or other phases were detected, demonstrating the high purity of the samples. Both anatase and rutile phases typically evolve from TiO_6 via octahedral rearrangement. It is widely accepted that phase rearrangement through edge-sharing favors the formation of the rutile phase (i.e., above 520°C), while the anatase phase is favored through rearrangement via corner-sharing below 520 °C [13]. The mean crystallite size of SG, SG-H, SG-L, and SG-L-H was calculated to be 24.37, 24.36, 9.81, and 7.89 nm, respectively (Table 1), using (1).

Table 1. Summary of results about the characterization of catalysts

Sample	SG	SG-H	SG-L	SG-L-H
Phase	Rutile	Rutile	Anatase	Anatase
BET (m^2/g)	0.95	18.95	82.65	168.59
Crystallite size (nm)	24.37	24.36	9.81	7.89
Eg (eV)	2.97	3.38	3.30	3.44

3.2. Morphology of Catalysts

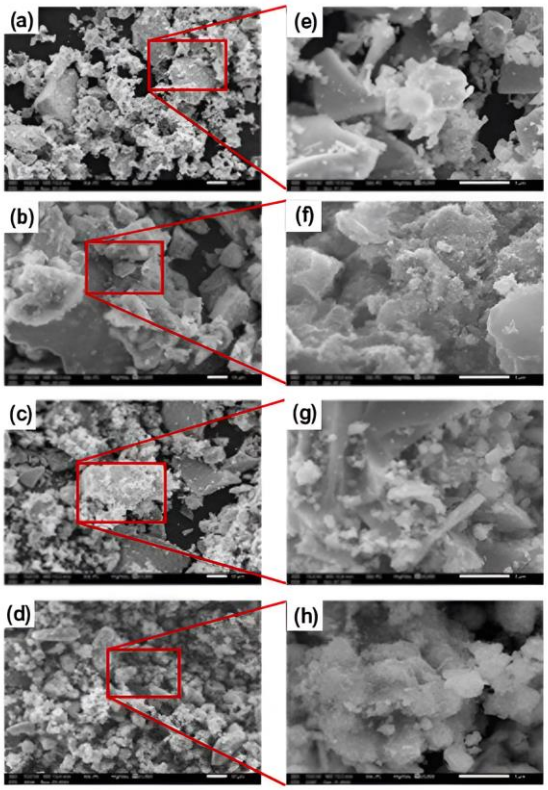

Fig. 7. SEM images of TiO_2 samples with x1000 magnification (a-d) and x5000 magnification (e-h) (with SG, SG-H, SG-L, and SG-L-H, respectively)

The morphology of TiO_2 catalyst particles was investigated by scanning electron microscopy (SEM) as illustrated in Fig. 7. All samples exhibited a micro-particle morphology. The morphology of rutile

TiO_2, which includes the SG and SG-H samples, is illustrated in Fig. 7a, b, e, and f. In contrast, the morphology of anatase TiO_2, including the SG-L and SG-L-H samples, is depicted in Figures 7c, d, g, and h. After hydrothermal, the particles tend to cluster together and decrease the size. The images of the four obtained samples are consistent with the XRD analysis, in which the samples (SG and SG-H) with dominant rutile phase show the formation of larger grain structures than the samples (SG-L and SG-L-H) with the dominant anatase phase. To further confirm the change in surface area after hydrothermal, the surface area measurement was conducted.

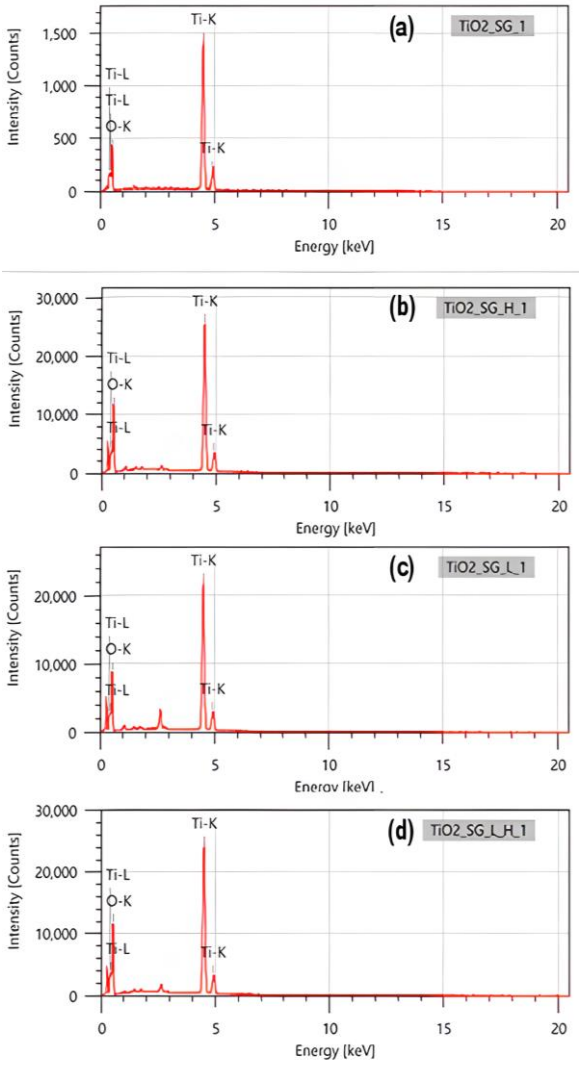

Fig. 8. EDS spectrum of synthesized TiO_2 by different methods: (a) SG, (b) SG-H, (c) SG-L, (d) SG-L-H

The elemental analysis of the synthesized TiO_2 particles was carried out and the results are shown in Fig. 8. The results show the strong signal intensities of Ti and O, indicating that the sample primarily contains TiO_2. There are also some small signals in the range of 1-3 eV with weak intensities, which may indicate noise during the analysis or a weak signal of impurities during the synthesis process. However, these do not affect the photoactivity of catalysts. To confirm that, let us follow the results of some photoactivity experiments performed on all TiO_2 samples in the next section.

Brunauer-Emmett-Teller (BET) surface area measurement was performed on the catalyst samples to compare specific surface areas and predict their adsorption capacity. The results of the surface area are shown in Table 1. As a result, the adsorption ability of catalysts is improved because of increasing their specific surface area by the hydrothermal treatment.

The SG-L catalyst sample synthesized at low-temperature gives a good specific surface area (82.65 m^2/g), which is larger than the sample (SG) synthesized by the traditional sol-gel method. From the observation of SEM images and BET results, it can be seen that the TiO_2 particles after hydrothermal treatment have a smaller particle size and a larger specific surface area. Hydrothermal treatment often increases the surface area. As a result, the adsorption process of pollutants onto the catalyst is faster and the photocatalytic activity is improved. UV-DRS measurement and the photocatalytic degradation of MB dye were conducted to clarify this further.

Fig. 9 shows the UV-DRS of TiO_2 samples. All of samples represent the TiO_2 absorption band in the ultraviolet region (about 375 nm).

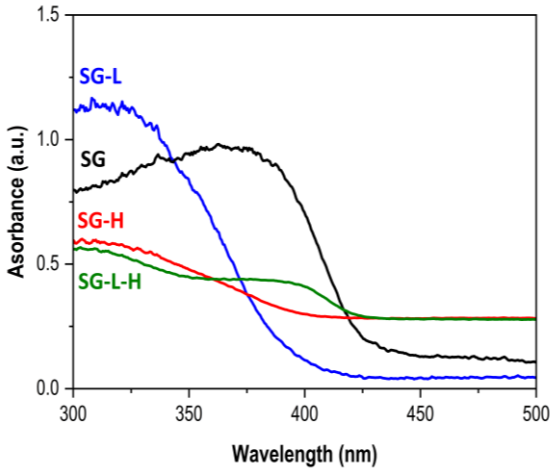

Fig. 9. UV-DRS of TiO_2 samples

Additionally, we determined the optical band gap energy of TiO_2 samples from the Tauc's equation [15]:

$$(\alpha h\nu)^{1/2} = A(h\nu - E_g) \quad (4)$$

in which α is the absorption coefficient, $h\nu$ is the photon energy, E_g is the optical bandgap energy, and A is a constant depending on the nature of the material. In the Tauc plot in Fig. 10, the optical band gap

energies of the SG, SG-H, SG-L, and SG-L-H TiO_2 particles were to be 2.97, 3.38, 3.33, and 3.44 eV, respectively. It can be seen that the optical band gap decreased with an increase in crystallite size.

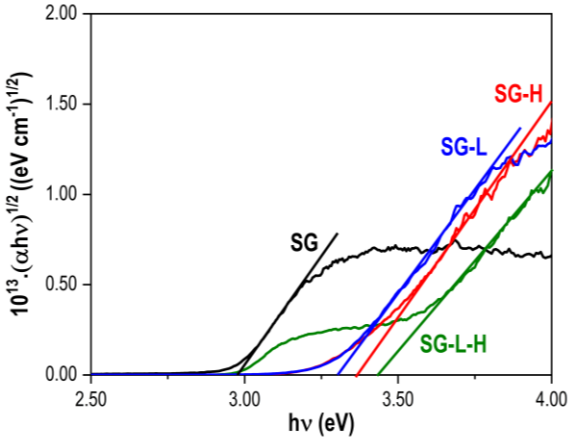

Fig. 10. Tauc plots obtained from Tauc's equation, $(\alpha h\nu)^{1/2}$ as a function of energy ($h\nu$) to determine the indirect bandgap energies of TiO_2 samples

3.3. Photoactivity of Catalysts

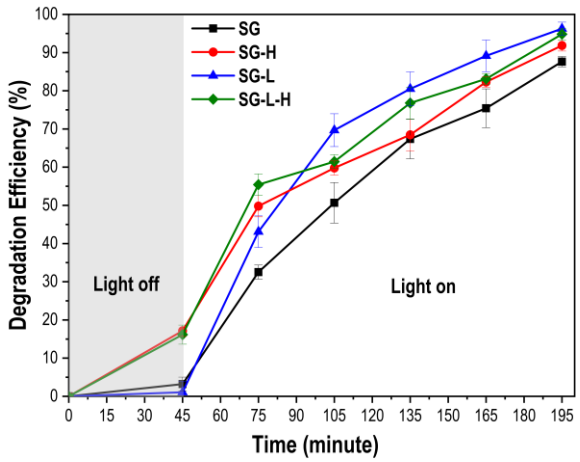

Fig. 11. Degradation efficiency MB of TiO_2 samples under the illumination of Xenon lamp

Fig. 11 shows the ability of TiO_2 samples to adsorb MB molecules on their surface in the absence of light exposure and to exhibit photocatalytic activity under illumination.

The catalyst particles synthesized via the hydrothermal method demonstrated significantly higher adsorption capabilities–compared to the two samples that were not hydrothermally treated. The increase in specific surface area enhanced the MB adsorption capacity. Specifically, the order of specific surface area is SG < SG-L < SG-H < SG-L-H, which corresponds to the increase in MB adsorption capacity of SG and SG-L (<5%) compared to SG-L-H and SG-H (about 20%). In terms of the photocatalytic process, the bandgap energy of the SG-L and SG-L-H samples (as determined by UV-DRS) is lower than that of SG and SG-H, leading to better MB degradation efficiency on SG-L than SG and SG than SG-H. In many previous studies, the bandgap energy on TiO_2 with the anatase phase is found to be lower than that of the rutile phase, which is consistent with the phase composition results on XRD patterns [16]. This aligns with SEM imaging predictions and BET measurements, which indicated an increased catalyst surface area following hydrothermal treatment.

The photocatalytic activity of the TiO_2 samples was evaluated by their ability to degrade MB under the influence of UV light from a Xenon lamp. As the exposure time increased, TiO_2 received more light, resulting in an increased production of highly oxidative free radicals that effectively decomposed MB molecules. Approximately 97% of the initial dye was degraded by the single-phase anatase samples (SG-L, SG-L-H) and achieved the highest MB degradation efficiency within 150 minutes. In contrast, the single-phase rutile samples (SG, SG-H) only achieved approximately 87% MB degradation under the same period of illumination. Anatase TiO_2 exhibits enhanced photoactivity compared to rutile in the degradation of organic pollutants and disinfecting water. This MB degradation efficiency result is consistent with the calculated band gap values for the catalysts, where catalysts with smaller band gap values require lower energy input (corresponding to light with larger wavelengths) to separate electrons (e^-) from holes (h^+), leading to the easy formation of important OH• radicals. Additionally, the crystal structure of anatase provides a greater density of active surface sites, promoting stronger interactions with target molecules. This increased surface reactivity leads to improved catalytic efficiency, making anatase an attractive choice for processes involving pollutant degradation, water purification and air treatment.

3.4. Kinetics of MB Degradation by TiO_2

The rate and kinetics of MB removal are compared using the zero-order (5), pseudo first-order (6), and pseudo second-order kinetic (7) models.

Pseudo zero-order: $C_t = k_0 t + C$ (5)

Pseudo first-order: $ln\frac{C_0}{C_t} = k_1 t$ (6)

Pseudo second-order: $\frac{1}{C_t} = \frac{1}{C_0} + k_2 t$ (7)

where C_0 is the initial concentration of MB (ppm), C_t is the concentration of MB at time t (ppm), t is the contact time in minutes, and k_0, k_1, k_2 are zero-order, first-order and second-order rate constant, respectively [17].

Fig. 12 corresponds to the kinetics model fitted for the pseudo zero-order, first-order, and second-order models at MB 10 ppm, respectively.

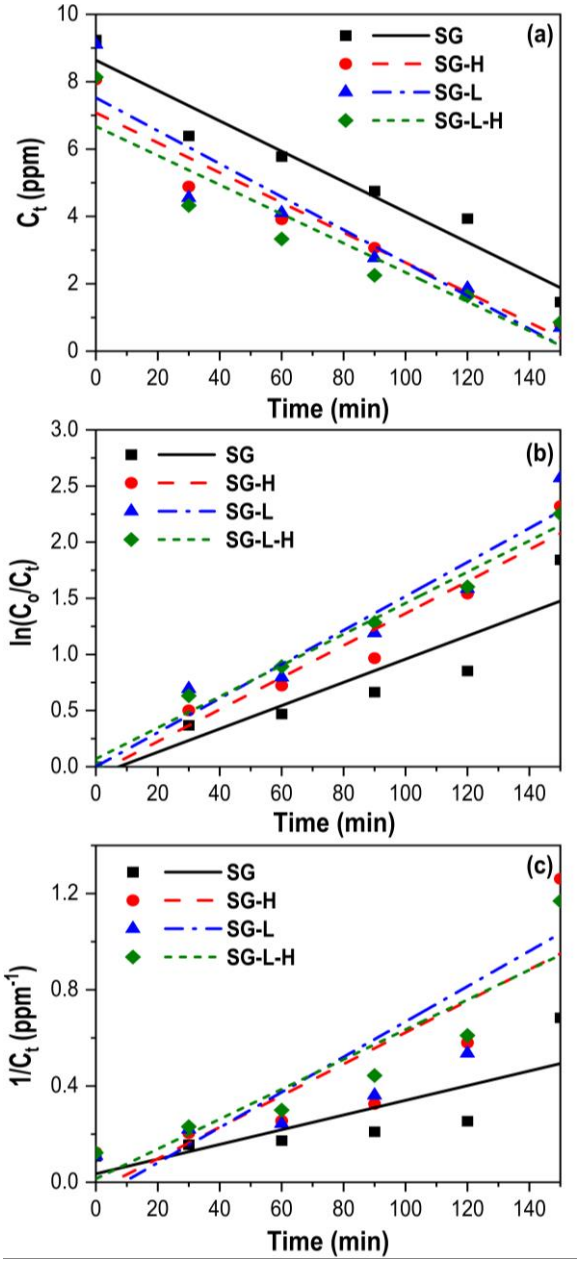

Fig. 12. Kinetic plot for MB degradation (a) zero-order (b) first-order (c) second-order models of TiO_2 samples

Table 2 summarizes the rate constant *K* and its regression coefficient for the models under discussion. The pseudo-first-order model with the best regression gave a better fit compared to the zero-order and second-order models. Therefore, the removal rate of MB onto the TiO_2 catalyst follows the pseudo first-order kinetic model as a function of the initial concentration of MB onto the TiO_2 catalyst follows the first-order kinetic model as a function of the initial concentration of MB. According to Table 2, SG-L has the highest rate of reaction (K_1 = 0.016) and the best photoactivity, which is suitable for the above results.

4. Conclusion

TiO_2 nanoparticles were successfully synthesized using various approaches for the degradation of organic dye MB. The structural and phase characteristics of the catalyst particles were verified by XRD and SEM analysis. Notably, hydrothermal treatment significantly enhanced the specific surface area of the catalyst, increasing from 0.95 to 18.95 m^2/g with the sol-gel method and from 82.65 to 168.59 m^2/g with the sol-gel low-temperature, which has been proven through BET measurement. The photocatalytic decomposition of MB was applied to study the photoactivity of TiO_2 catalyst samples. TiO_2 anatase synthesized via the sol-gel low-temperature method and hydrothermal sol-gel low-temperature method exhibited the best photoactivity, achieving over 97% decomposition of MB after 150 minutes under the illumination of a Xenon lamp. In comparison, the TiO_2 rutile samples, produced through the sol-gel and hydrothermal sol-gel methods, exhibited a decomposition efficiency of approximately 87% under similar illumination conditions. Therefore, we conclude that the sol-gel low-temperature method is the most effective approach, as it not only produces highly active catalytic particles but is also straightforward and easy to implement.

Acknowledgments

This research is funded by Hanoi University of Science and Technology (HUST) under project number T2023-PC-107.

This research was a part supported by RoHan Project for some measurements that funded by the German Academic Exchange Service (DAAD, No. 57315854) and the Federal Ministry for Economic Cooperation and Development (BMZ) inside the framework "SDG Bilateral Graduate School Programme".

Table 1. Kinetic parameters for photocatalytic removal of MB of TiO_2 samples

Order of reaction	Paraments	Units	SG	SG-H	SG-L	SG-L-H
Pseudo zero-order	K_0	$mg.L^{-1}.min^{-1}$	0.045	0.044	0.049	0.043
	R^2		0.930	0.937	0.843	0.833
Pseudo first-order	K_1	min^{-1}	0.009	0.014	0.016	0.015
	R^2		0.924	0.979	0.975	0.993
Pseudo second-order	K_2	$mg^{-1}.L.min^{-1}$	0.003	0.005	0.007	0.006
	R^2		0.853	0.877	0.837	0.937

References

[1] H. N. C. Dharma *et al.*, A review of titanium dioxide (TiO_2)-based photocatalyst for oilfield-produced water treatment, Membranes, vol. 12, no. 3, pp. 345, Mar. 2022. https://doi.org/10.3390/membranes12030345

[2] S. M. Tichapondwa, J. Newman, and O. Kubheka, Effect of TiO_2 phase on the photocatalytic degradation of methylene blue dye, Physics and Chemistry of the Earth, part A/B/C, vol. 118-119, pp. 102900, Oct. 2020. https://doi.org/10.1016/j.pce.2020.102900

[3] D. Bokov *et al.*, Nanomaterial by sol-gel method: synthesis and application, Advances in Materials Science and Engineering, vol. 2021, iss. 1, Dec. 2021. https://doi.org/10.1155/2021/5102014

[4] S. Mathew Simon *et al.*, Recent advancements in multifunctional applications of sol-gel derived polymer incorporated TiO_2-ZrO_2 composite coatings: a comprehensive review, Applied Surface Science, vol. 6, pp. 100173, Dec. 2021. https://doi.org/10.1016/j.apsadv.2021.100173

[5] B. Koozegar Kaleji and M. Gorgani, Comparison of sol-gel and hydrothermal synthesis methods on the structural, optical and photocatalytic properties of Nb/Ag codoped TiO_2 mesoporous nanoparticles, International Journal of Environmental Analytical Chemistry, vol. 102, iss. 14, pp. 3357-3372, May. 2022. https://doi.org/10.1080/03067319.2020.1767096

[6] O. Sadek *et al.*, Synthesis by sol-gel method and characterization of nano-TiO_2 powders, Materials Today Proceedings, vol. 66, pp. 456-458, Jan. 2022. https://doi.org/10.1016/j.matpr.2022.06.385

[7] D. J. A. Ahmed, B. I. Al-abdaly, and S. J. Hussein, Synthesis and characterization of high surface area nano titanium dioxide, Journal of Petroleum Research and Studies, vol. 11, no. 4, pp. 51-75, Dec. 2021. http://doi.org/10.52716/jprs.v11i4.563

[8] M. M. Ahmad, S. Mushtaq, H. S. Al Qahtani, A. Sedky, and M. W. Alam, Investigation of TiO_2 nanoparticles synthesized by sol-gel method for effectual photodegradation, oxidation and reduction reaction, Crystals, vol. 11, iss. 12, pp. 1456, Nov. 2021. https://doi.org/10.3390/cryst11121456

[9] N. S. Kumar, S. N. Kumar, and L. Yesappa, Structural, optical and conductivity study of hydrothermally synthesized TiO_2 nanorods, Materials Research Express, vol. 7, no. 1, pp. 015071, Jan. 2020. https://doi.org/10.1088/2053-1591/ab691f

[10] E. A. Rosdiana, N. B. A. Prasetya, and G. Gunawan, Synthesis and characterization of TiO_2-chitosan beads and its application as a degradation agent of methylene blue, Trends Sciences, vol. 20, no. 9, pp. 6670-6670, Apr. 2023. https://doi.org/10.48048/tis.2023.6670

[11] I. Oshina and J. Spigulis, Beer-Lambert law for optical tissue diagnostics: current state of the art and the main limitations, Journal of Biomedical Optics, vol. 26, iss. 10, pp. 100901-100901, Oct. 2021. https://doi.org/10.1117/1.JBO.26.10.100901

[12] E. Paradisi, P. J. Plaza-González, G. Baldi, J. M. Catalá-Civera, and C. Leonelli, On the use of microwaves during combustion/calcination of *N*-doped TiO_2 precursor: an EMW absorption study combined with TGA-DSC-FTIR results, Materials Letters, vol. 338, pp. 133975, May. 2023. https://doi.org/10.1016/j.matlet.2023.133975

[13] M. Benčina, A. Iglič, M. Mozetič, and I. Junkar, Crystallized TiO_2 nanosurfaces in biomedical applications, Nanomaterials, vol. 10, iss. 6, pp. 1121, Jun. 2020. https://doi.org/10.3390/nano10061121

[14] M. Lal, P. Sharma, and C. Ram, Calcination temperature effect on titanium oxide (TiO_2) nanoparticles synthesis, Optik, vol. 241, pp. 166934, Sep. 2021. https://doi.org/10.1016/j.ijleo.2021.166934

[15] A. Al-Muntaser *et al.*, Boosting the optical, structural, electrical, and dielectric properties of polystyrene using a hybrid GNP/Cu nanofiller: novel nanocomposites for energy storage applications, Journal of Materials Science: Materials in Electronics, vol. 34, no. 7, pp. 678, Mar. 2023. http://dx.doi.org/10.1007/s10854-023-10104-7

[16] S. F. Lee, E. D. H. Kong, J. H. F. Chau, K. M. Lee, and C. W. Lai, Enhanced acetaminophen photodegradation under UV using anatase-rutile TiO_2 phase heterojunction - Z-scheme mechanism and factors affecting efficiency, Journal of Photochemistry and Photobiology A: Chemistry, vol. 456, pp. 115844, Nov. 2024. https://doi.org/10.1016/j.jphotochem.2024.115844

[17] V. Duarte Leite, R. Ramos, P. Silva, W. Lopes, and J. Sousa, Kinetic models describing the hydrolytic stage of the anaerobic co-digestion of solid vegetable waste and anaerobic sewage sludge, Biomass Conversion and Biorefinery, vol. 13, no. 13, pp. 343-353, May. 2021. https://doi.org/10.1007/s13399-021-01574-y